

Towards a Robust Exclusion of the Sterile-Neutrino Explanation of Short-Baseline Anomalies

Ohana Benevides Rodrigues,^{1,*} Matheus Hostert,^{2,†} Kevin J. Kelly,^{3,‡} Bryce Littlejohn,^{1,§} Pedro A. N. Machado,^{4,¶} Ibrahim Safa,^{5,**} and Tao Zhou^{3,††}

¹*Department of Physics, Illinois Institute of Technology, Chicago, Illinois 60616*

²*Department of Physics & Laboratory for Particle Physics and Cosmology, Harvard University, Cambridge, MA 02138, USA*

³*Department of Physics and Astronomy, Mitchell Institute for Fundamental Physics and Astronomy, Texas A&M University, College Station, TX 77843, USA*

⁴*Theoretical Physics Department, Fermilab, P.O. Box 500, Batavia, IL 60510, USA*

⁵*Columbia University, New York, NY, 10027, USA*

(Dated: March 19, 2025)

The sterile neutrino interpretation of the LSND and MiniBooNE neutrino anomalies is currently being tested at three Liquid Argon detectors: MicroBooNE, SBND, and ICARUS. It has been argued that a degeneracy between $\nu_\mu \rightarrow \nu_e$ and $\nu_e \rightarrow \nu_e$ oscillations significantly degrades their sensitivity to sterile neutrinos. Through an independent study, we show two methods to eliminate this concern. First, we resolve this degeneracy by including external constraints on ν_e disappearance from the PROSPECT reactor experiment. Second, by properly analyzing the full three-dimensional parameter space, we demonstrate that the stronger-than-sensitivity exclusion from MicroBooNE alone already covers the entire 2σ preferred regions of MiniBooNE at the level of $2 - 3\sigma$. We show that upcoming searches at SBND and ICARUS can improve on this beyond the 4σ level, thereby providing a rigorous test of short-baseline anomalies.

Introduction – For decades, measurements of neutrino interactions have presented unexpected results, leading to new interpretations of the Standard Model (SM) of particle physics and beyond. In one such case, the MiniBooNE experiment (heretofore, MB) observed a significant excess (4.8σ above backgrounds) of electron-neutrino-like events at low energies [1], still to be resolved. This excess, which has thus far not been explained by conventional neutrino-nucleus interactions or unknown backgrounds [2–5], has prompted extensive theoretical and experimental investigations [6] and bears significant implications for particle physics and cosmology.

The simplest interpretation of this anomaly involves eV-scale sterile neutrinos – SM-singlet fermions that can mix with active neutrinos driving short-baseline oscillations. This interpretation is also historically what connected MiniBooNE to the anomalous results of the Liquid Scintillator Neutrino Detector (LSND) experiment [7], a 3.8σ excess of $\bar{\nu}_e$ events in a neutrino source from μ^+ decays at rest. While global fits involving dozens of experiments have established a tension between these anomalies and other results [8–10], direct tests of the MiniBooNE anomaly using experiments with similar neutrino beams and energy ranges can provide particularly valuable insights into the nature of the excess.

The MicroBooNE experiment (μ B) was specifically designed to test the MB anomaly using the superior particle identification capabilities of liquid argon time projection chamber (LArTPC) technology [11]. Operating in the same neutrino beam as MB, the Booster Neutrino Beam, μ B can distinguish between electron-like events and other backgrounds such as single photons and π^0 with unprece-

dedented precision [12–16]. This enhanced background discrimination significantly reduces systematic uncertainties associated with photon-related backgrounds, which were an important source of uncertainty in the MB analysis [3, 17].

Recent sterile-neutrino analyses have supported the idea that μ B data remain compatible with MB’s allowed region [18–20]. Three sterile-neutrino parameters govern oscillations relevant to MB and μ B: two mixing angles and a mass-squared splitting Δm_{41}^2 . The mixing elements U_{e4} and $U_{\mu 4}$ individually control ν_e and ν_μ disappearance, while their product determines the appearance probability through $\sin^2(2\theta_{\mu e}) \equiv 4|U_{e4}|^2|U_{\mu 4}|^2$. The copious ν_μ events are often used as a control sample to mitigate flux and cross section uncertainties. However, the Booster Neutrino Beam contains an intrinsic component of ν_e , at the level of 0.5%, representing a significant background to appearance searches. This background introduces an inescapable degeneracy between $\nu_\mu \rightarrow \nu_e$ appearance and $\nu_e \rightarrow \nu_e$ disappearance signals for some combination of mixing parameters.

We show here that when profiling over a multi-dimensional parameter space and showing allowed regions in $\sin^2(2\theta_{\mu e})$ versus Δm_{41}^2 , comparisons between different experiments can be misleading. Difficulties arise from the fact that, for a common $\sin^2(2\theta_{\mu e})$ point in this parameter space, two experiments’ underlying best-fit parameters $|U_{e4}|^2$ and $|U_{\mu 4}|^2$ need not be the same. By examining the full three-dimensional parameter space ($|U_{e4}|^2, |U_{\mu 4}|^2, \Delta m_{41}^2$), we reveal stronger tensions between MB and μ B than previously recognized. Our analysis accounts for how these parameters influence the con-

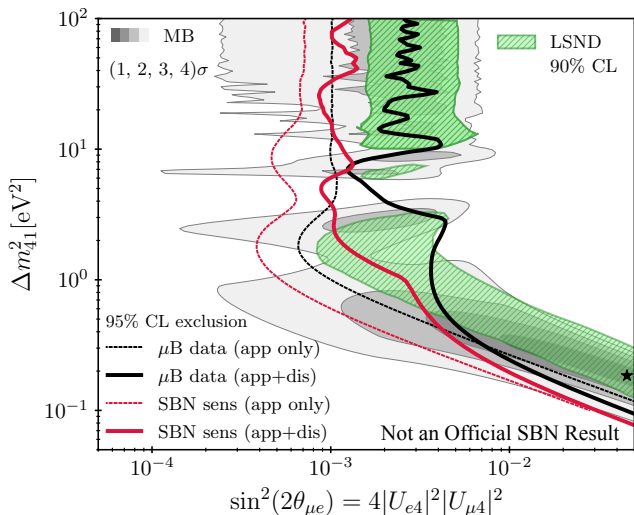


FIG. 1. The sterile neutrino parameter space and 1, 2, 3, 4 σ preferred regions of MiniBooNE (grey regions) and 90% CL region of LSND (green region) along with the 95% CL MicroBooNE exclusion (black lines) and SBN sensitivity (red lines), assuming Wilks’ theorem. Solid lines show the result of a full 3 + 1 oscillation model and dashed lines of the common but physically-inconsistent, appearance-only model. The MiniBooNE fit is shown for the full oscillation model. For LSND, they are approximately the same. The apparent compatibility between experiments is a potential artifact of the projection into the appearance mixing angle.

control sample and background predictions in both MB and μ B. We demonstrate that μ B can rule out MB’s entire 2 σ preferred region at more than 95% confidence level when properly accounting for all parameter correlations. We also examine how sterile-neutrino exclusion is improved when considering electron-flavor disappearance data from the reactor-based PROSPECT experiment constraints and future data from the Fermilab SBN program – both in terms of profiled $\sin^2(2\theta_{\mu e})$ - Δm_{41}^2 space and the un-profiled full three-dimensional parameter space.

Short-baseline Oscillations & Degeneracies –

The sterile neutrino interpretation of the MB anomaly requires extending the standard three-neutrino framework to include a fourth mass eigenstate. At short baselines, the oscillation probabilities in this framework take a simple form. The appearance probability is given by

$$P(\nu_\mu \rightarrow \nu_e) = \sin^2(2\theta_{\mu e}) \sin^2\left(\frac{\Delta m_{41}^2 L}{4E}\right), \quad (1)$$

while for disappearance

$$P(\nu_\alpha \rightarrow \nu_\alpha) = 1 - \sin^2(2\theta_{\alpha\alpha}) \sin^2\left(\frac{\Delta m_{41}^2 L}{4E}\right), \quad (2)$$

where $\sin^2(2\theta_{\alpha\alpha}) \equiv 4|U_{\alpha 4}|^2(1 - |U_{\alpha 4}|^2)$ for $\alpha = e, \mu$.

In short-baseline oscillation experiments, such as MB and μ B, intrinsic ν_e backgrounds are affected by the same mixing parameters that control appearance. The ν_e disappearance probability scales with U_{e4} , partially compensating any appearance signal. Additionally, the ν_μ flux used to predict the appearance signal is inferred from ν_μ measurements, which themselves can be depleted by oscillations from nonzero $U_{\mu 4}$. This interplay between appearance, disappearance, and flux determination introduces degeneracies with (potentially) different manifestations in each experiment’s parameter space.

The detector technologies employed by MB and μ B lead to different background compositions. MB’s Cherenkov detector cannot distinguish electrons from single photons that convert to e^+e^- pairs inside the fiducial volume, making π^0 decays and $\Delta(1232) \rightarrow \gamma N$ processes significant backgrounds. The LArTPC technology of μ B allows to distinguish electrons from photons using the presence of a gap between the event vertex and the electromagnetic shower, as well as the ionization yield in the first few centimeters of the shower, substantially reducing photon-related backgrounds. These different background compositions translate into different degeneracies in the sterile neutrino parameter space, which is crucial to estimate the compatibility between these two experiments, as we will see shortly.

Datasets and Simulations – We analyze MiniBooNE and MicroBooNE data using their data releases [14, 21], treating backgrounds consistently within the 3+1 oscillation framework. To estimate the sensitivity of the SBN program, we build on our existing μ B framework [18, 22]. Complementary electron neutrino disappearance constraints from the PROSPECT reactor neutrino experiment are also examined in this study. The PROSPECT experiment deployed a 4 ton segmented liquid scintillator detector target a distance of 7-9 meters from the High Flux Isotope Reactor (HFIR) at Oak Ridge National Laboratory [23], detecting over 60,000 inverse beta decay interactions ($\bar{\nu}_e + p \rightarrow e^+ + n$) while searching for short-baseline $\bar{\nu}_e$ disappearance [24, 25]. Rather than re-analyzing PROSPECT neutrino and background datasets, we use maps of $\Delta\chi^2$ versus $\sin^2(2\theta_{ee})$ and Δm_{41}^2 provided by PROSPECT in their final oscillation analysis using the full dataset from the now-decommissioned PROSPECT-I detector [26].

Pitfalls of Projection – Traditional sterile neutrino searches for anomalous $\nu_\mu \rightarrow \nu_e$ appearance – particularly LSND, MB, and μ B – present their results in the $\sin^2(2\theta_{\mu e})$ - Δm_{41}^2 plane, as we show in Fig. 1. While optimal for experiments that are sensitive almost exclusively to $\nu_\mu \rightarrow \nu_e$ appearance signals like LSND, this projection obscures important physical effects in experiments with significant neutrino-related backgrounds like MB and μ B. The latter experiments are sensitive not just to the product $4|U_{e4}|^2|U_{\mu 4}|^2$ via the appearance channel, but to individual mixing elements through ν_μ disappearance in

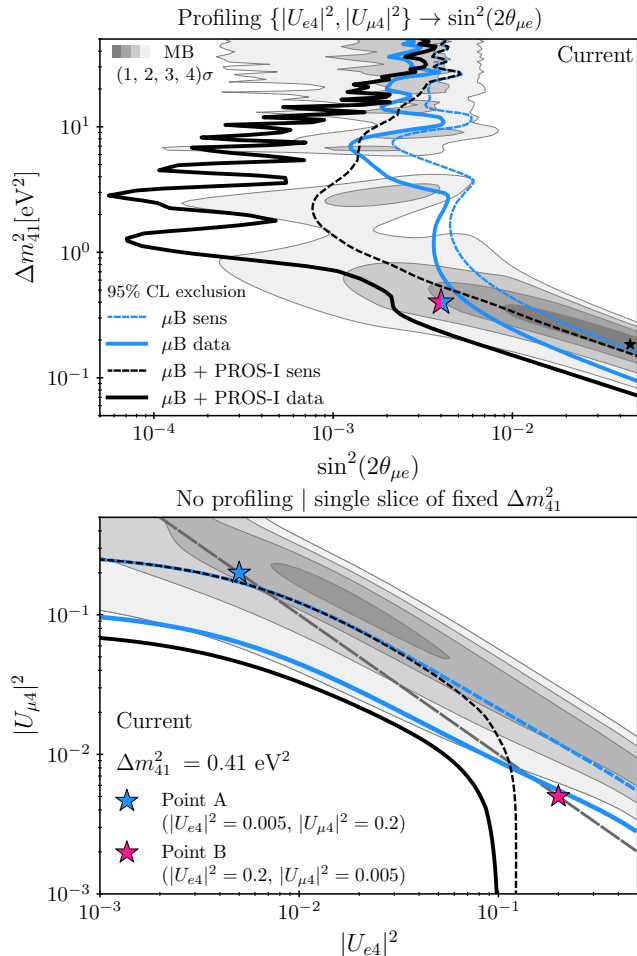


FIG. 2. Top) Typical sterile-neutrino parameter space presentation, comparing the MiniBooNE-preferred regions (grey), with 95% CL sensitivity/exclusion of MicroBooNE in blue (+PROSPECT in black), assuming Wilks’ theorem. Exclusions (data) are presented as thick, solid lines; sensitivities with thin, dashed lines.

Bottom) Slice of $\Delta m_{41}^2 = 0.41 \text{ eV}^2$ parameter space, allowing $\{|U_{e4}|^2, |U_{\mu4}|^2\}$ to vary independently *before profiling*. Blue (A) and red (B) stars both correspond to $\sin^2(2\theta_{\mu e}) = 4 \times 10^{-3}$ in the top panel. Despite this angle not being covered by μB in the profiled, top panel, the line it represents in the bottom panel contains no points compatible with *both* MB and μB .

flux-normalizing control samples and ν_e disappearance in backgrounds. Due to this scaling, a small appearance signal is typically accompanied by much larger disappearance effects. This leads to a nontrivial degeneracy among the mixing elements and the appearance amplitude.

Fig. 1 illustrates the impact of the above degeneracy: both μB and SBN sensitivities assuming the unphysical scenario of appearance-only oscillations are significantly stronger than in the full 3+1 model, which accounts for oscillations in the backgrounds and control sample. Within the consistent treatment of oscillations, this result naïvely suggests that there currently is a large

parameter space where concordance between MB and μB can be found and that SBN may not even be able to cover the entire 3σ region of the MB parameter space at more than 95% CL. However, as we show below, this conclusion is incorrect.

One avenue to reduce the impact of the degeneracy is to include data from a neutrino source with a different composition in terms of its ν_e/ν_μ flavor ratio. This is present in the NuMI beam and is currently being pursued by the μB collaboration [27, 28]. Indeed, the measurement of this flux at MiniBooNE [29] has already been used to constrain oscillations in Ref. [9], although, by itself, it is not very sensitive to sterile neutrinos. With a larger ν_e/ν_μ flavor ratio, appearance and disappearance signals can be directly constrained, and parameters for which ν_e disappearance can accommodate a greater amount of $\nu_\mu \rightarrow \nu_e$ appearance in the BNB flux without leading to an observable excess would not necessarily do so for the NuMI dataset, thereby reducing the impact of the degeneracy shown in Fig. 1.

The flavor-pure flux of $\bar{\nu}_e$ emanating from a nuclear reactor also offers an opportunity for reducing degeneracy in oscillation results from mixed-flavor neutrino beams. In Fig. 2(top) we present the μB exclusion in this parameter space with and without PROSPECT data. PROSPECT provides invaluable direct constraints on $|U_{e4}|^2$ through searches for short-baseline $\bar{\nu}_e$ disappearance. The combination of appearance and disappearance experiments naturally resolves the degeneracy in the 3+1 framework by directly imposing a limit on the amount of ν_e disappearance that is permissible in the intrinsic background, effectively removing the possibility to hide appearance signals. Combined with PROSPECT, the BNB experimental searches recover their constraining power in the traditional profiled parameter space of Figs. 1 and 2.

We note that the external PROSPECT constraints accentuates the difference between μB ’s sensitivity and exclusion: the constraint on $\sin^2(2\theta_{\mu e})$ for some values of Δm_{41}^2 is almost an order of magnitude stronger than the expected sensitivity. This is due to three contributing factors. First, the observed excess of ν_μ events at μB disfavors ν_μ disappearance. Second, and more importantly, the accompanying observed deficit of ν_e events leaves less room for $\nu_\mu \rightarrow \nu_e$ appearance. Finally, upon accounting for external constraints on ν_e disappearance from PROSPECT, any amount of $\nu_\mu \rightarrow \nu_e$ appearance is strongly disfavored.

Apart from adding new datasets, another way to confront this degeneracy is to investigate the parameter space without relying on profiling over unseen parameters. To illustrate this point, we take two benchmark points with the same appearance angle $\sin^2(2\theta_{\mu e}) = 0.004$ and mass splitting $\Delta m_{41}^2 = 0.41 \text{ eV}^2$ but different mixing patterns: (A) $|U_{e4}|^2 = 0.005$ and $|U_{\mu4}|^2 = 0.2$ and (B) $|U_{e4}|^2 = 0.2$ and $|U_{\mu4}|^2 = 0.005$. In the top panel of Fig. 2, these two points appear as the half-blue/half-pink

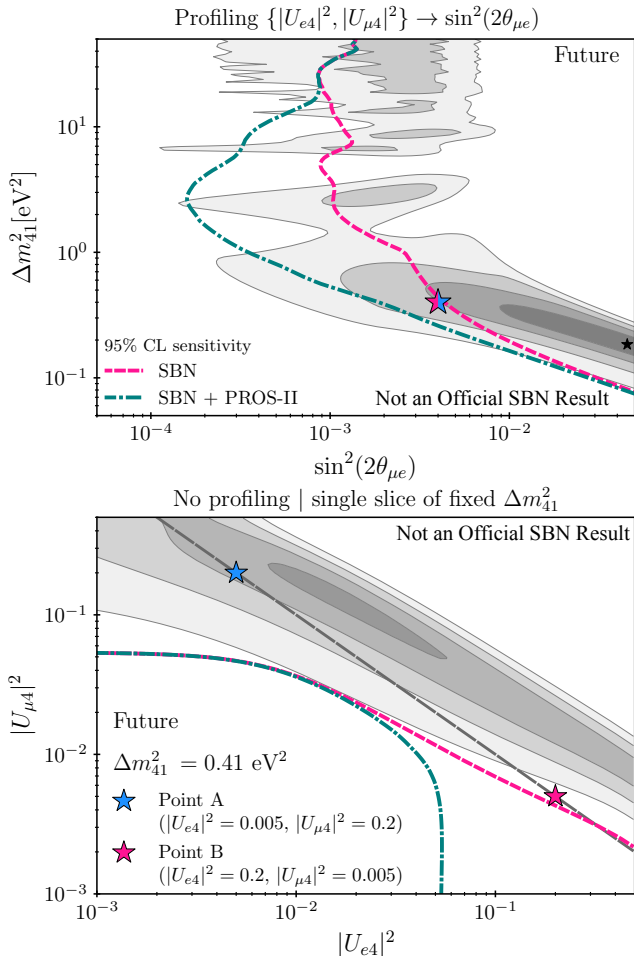


FIG. 3. Same as Fig. 2, focusing on future projections of SBN (pink) and SBN+PROSPECT-II (green) capabilities.

star, apparently compatible both with MB’s preference for the existence of a sterile neutrino and compatible with μ B’s null result – according to the profiled parameter space, μ B lacks the statistical power to meaningfully exclude this point. However, in the fixed- Δm_{41}^2 slice of the parameter space in the bottom panel, these two points are distinct and neither of them is simultaneously compatible with *both* MB and μ B. Indeed, the entire dashed gray line where $\sin^2(2\theta_{\mu e}) = 0.004$ in the slice panel collapses onto the star of the profiled plane, but nowhere along it can the preference regions of MB and μ B be simultaneously satisfied.

While our benchmark points (A) and (B) yield identical $\sin^2(2\theta_{\mu e})$, they produce distinct event rates in the ν_μ sample, and in the ν_e sample due to different background compositions. This is explicitly shown in Fig. 6 of the Endmatter, where we compare predicted event spectra for μ B’s ν_e and ν_μ samples, as well as MB electron-like events. The relatively large value of $|U_{\mu 4}|^2$ of point (A) is disfavored by μ B as it significantly affects the ν_μ

channel. Point (B), on the other hand, has a smaller value of $|U_{\mu 4}|^2$, barely changing ν_μ disappearance, and is allowed by μ B data. Nevertheless, the larger value of $|U_{e 4}|^2$ leads to too much disappearance of the intrinsic ν_e background, not providing enough excess of electron-like events in MB to be favored by the data.

The aforementioned degeneracy is therefore effectively broken, and a fundamental tension between μ B and MB is revealed in the full three-dimensional parameter space of sterile neutrinos that would otherwise remain obscured in traditional profiled comparisons. This point is demonstrated by Fig. 2(bottom) for a specific choice of Δm_{41}^2 , and is generalized for the broader parameter space in Fig. 5 of the Endmatter, where we show more slices of the parameter space for 3 degrees of freedom. While the profiled space provides a picture of potential consonance between MB and μ B at the chosen Δm_{41}^2 , the full space in Fig. 2 shows no overlap between the μ B 95% CL allowed region and MB’s 3σ allowed region. Adding PROSPECT excludes all of MB’s 4σ allowed region at this Δm_{41}^2 . Across the full phase space, we observe that no single combination of mixing parameters in the 3+1 scenario can simultaneously explain MB’s excess at 2σ while remaining consistent with μ B’s observations at the same confidence level.

Future Projections – With future data from SBND and ICARUS, the capability of excluding the three-dimensional MB-preferred parameter space is even stronger. To simulate these, we make the simplified assumption that SBND and ICARUS will have the same signal efficiency as μ B, as well as the same number of backgrounds per neutrino per fiducial mass. This is a conservative estimate, as SBND and ICARUS are expected to improve upon detector performance, event reconstruction, and analysis techniques [30, 31]. With our procedure, SBND and ICARUS share the same energy binning and resolution as the μ B analysis discussed above. We take the fiducial mass to be 112 t and 476 t of liquid argon for SBND and ICARUS, respectively, with a total exposure of 6.6×10^{20} POT. The neutrino flux at the location of SBND and ICARUS is rescaled from the μ B flux by an overall energy-independent factor of $(L_{\mu B}/L_{\text{SBND/ICARUS}})^2$, where $L_{\text{SBND}} = 110$ m, $L_{\text{ICARUS}} = 600$ m, and $L_{\mu B} = 470$ m are the approximate detector distances to the target. More details can be found in the Endmatter. Projecting forward, we also consider future reactor antineutrino observations from PROSPECT-II. We use $\Delta\chi^2$ maps provided by the collaboration that describe the expected sensitivity of a two-year run at HFIR with an upgraded detector [32].

In Fig. 3, we present the same comparison of MB-preferred parameter space against future projections including SBN and additionally PROSPECT-II. In the top panel, the (misleading) profiling of $\{|U_{e 4}|^2, |U_{\mu 4}|^2\} \rightarrow \sin^2(2\theta_{\mu e})$ portrays sensitivity that is not as impres-

sive as one would hope – the SBN-only and SBN + PROSPECT-II projections only demonstrate modest improvement on the current μB and μB + PROSPECT results.¹ In contrast, when we focus on the sliced parameter space (bottom panel of Fig. 3 along with projections in Fig. 5 of the Endmatter), the future improvements are readily apparent. Across the three-dimensional parameter space $\{|U_{e4}|^2, |U_{\mu4}|^2, \Delta m_{41}^2\}$, SBN and PROSPECT-II will thoroughly explore the MB-preferred parameter space.

Compatibility with MiniBooNE – To quantify the compatibility between any given null results and the MB-preferred multi-dimensional space, we construct a compatibility χ^2 . For a given value $\Delta\chi_0^2$, we obtain the 3D region in the sterile neutrino parameter space satisfying $\Delta\chi_{\text{MB}}^2 < \Delta\chi_0^2$. Then, scanning that entire region, we quantify the minimum $\Delta\chi_{\text{exp}}^2$ of another experiment within that region – determining the level at which that experiment excludes the entirety of the MB-preferred $\Delta\chi^2$ region.² This is presented for μB and its Asimov sensitivity expectation, and for the projection for SBN in Fig. 4.

Each curve’s intersection with the dashed grey diagonal line addresses the question: “at what confidence level X can this experiment exclude MB’s preference at the same confidence level?” This corresponds to $\Delta\chi^2 = 9.5$ for μB alone (compared to $\Delta\chi^2 = 4.8$ for its sensitivity), which increases modestly by adding PROSPECT. With three degrees of freedom and assuming Wilks’ theorem, this means μB excludes MB’s entire 2.3σ (97.6% CL) region at greater than the same confidence level. This should be contrasted with the compatibility calculated using the μB sensitivity, which yields 1.3σ (80.9% CL). This quantitative analysis confirms our parameter space exploration – no point in the full three-dimensional parameter space can simultaneously explain MB’s excess while remaining consistent with μB ’s observations at more than 2σ .³ We also see that SBN will improve on this substantially, covering the entire 3σ region of MB at more than 3σ while excluding MB’s most-favored $\sim 2\sigma$ parameter space with extremely high ($>5\sigma$) confidence.

Discussion – We have presented two complementary arguments that show that the MicroBooNE experiment and the SBN program will robustly cover the

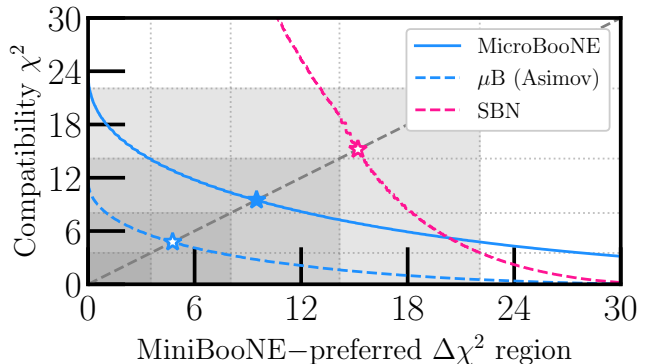


FIG. 4. The compatibility χ^2 of MicroBooNE (blue) and SBN (pink) compared against the MiniBooNE-preferred parameter space, as described in the text. Each experiment’s intersection with the diagonal grey line is of particular emphasis. Grey regions contain the regions of compatibility, assuming Wilks’ theorem, starting at 1σ (darkest grey) to 4σ (lightest grey).

sterile neutrino interpretation of the LSND and MiniBooNE anomalies. This is the first time that the MicroBooNE exclusion and the SBN sensitivities are shown throughout the full $3 + 1$ -oscillation model without resorting to the statistical procedure of profiling. In this full oscillation model, the coexistence of a $\nu_\mu \rightarrow \nu_e$ appearance signal and the disappearance of ν_e backgrounds and ν_μ in the control sample leads to a degeneracy and an apparent loss of experimental sensitivity to the model in the plane of $\sin^2(2\theta_{\mu e})$ vs Δm_{41}^2 , after profiling. We conclude, however, that when comparing allowed experimental regions *before* profiling, this effect does not substantially diminish the exclusion power of μB data – we were able to achieve this by generalizing the MiniBooNE, MicroBooNE, and SBN fits to slices of the full three-dimensional parameter space: $(|U_{e4}|^2, |U_{\mu4}|^2, \Delta m_{41}^2)$. Exploring the full three-dimensional parameter space provides qualitatively different conclusions. For this reason, we urge all experiments that are sensitive to multiple oscillation parameters to make their full multi-dimensional χ^2 maps available, including MiniBooNE, to enable these compatibility comparisons in the future by the SBN program.

Even in the profiled case, we show that the degeneracy in μB data can be avoided altogether by incorporating strong existing constraints on ν_e disappearance from the flavor-pure PROSPECT reactor neutrino dataset. Besides PROSPECT, constraints on electron-flavor disappearance from μB ’s NuMI beam datasets [27, 28] and from solar neutrino [33] and absolute reactor neutrino flux measurements [34–36], while not examined here, can play a complementary degeneracy-reducing role. When examining the full three-dimensional oscillation phase space, PROSPECT data unsurprisingly serves as the strongest constraint on large $|U_{e4}|$ values.

¹ This may, however, be driven by the fluctuations present in μB data relative to its expectations.

² More precisely, given a region of the model parameter space defined by $\vartheta(\Delta\chi_0^2) = \{\vartheta | \Delta\chi_{\text{MB}}^2 < \Delta\chi_0^2\}$, the compatibility χ^2 for a given experiment or set of experiments is defined as $\chi_{\text{exp}}^2(\Delta\chi_0^2) = \min_{\vartheta(\Delta\chi_0^2)} \{\Delta\chi_{\text{exp}}^2\}$.

³ The addition of PROSPECT data for improving this exclusion is only modest: μB + PROSPECT excludes MB’s entire 2.4σ (98.5% CL) at greater than the same confidence level. In contrast, the Asimov-expected exclusion of μB + PROSPECT is 1.7σ (91.3% CL).

Finally, we construct a quantitative measure of the statistical compatibility between any combination of experiments, and illustrate it for MiniBooNE, MicroBooNE, PROSPECT, and SBN in the sterile neutrino model. By requiring no overlap between the region of preference of MiniBooNE with that of MicroBooNE, we conclude that under this metric, the compatibility between these two experimental results is at the level of $\chi^2 \sim 10$, corresponding to just above 2σ statistical incompatibility. Generalizing this result to SBN, we find that eventually the SBN program could drive this compatibility metric to the level of $\chi^2 = 16$, or just above 3σ , while excluding MB's most-favored parameter space with extremely high ($>5\sigma$) confidence.

Acknowledgements: We thank Joachim Kopp for comments on this manuscript. The work of MH is supported by the Neutrino Theory Network Program Grant #DE-AC02-07CHI11359 and the US DOE Award #DE-SC0020250. KJK and TZ are supported in part by US DOE Award #DE-SC0010813. OBR and BRL are supported by US DOE Award #DE-SC0008347. The work of IS was supported by the National Science Foundation Award PHY-2310080. This manuscript has been authored by Fermi Forward Discovery Group, LLC under Contract No. 89243024CSC000002 with the U.S. Department of Energy, Office of Science, Office of High Energy Physics.

Note: This work is not an official MicroBooNE, SBND, or ICARUS result.

ENDMATTER

Full slices of parameter space – In this appendix we expand on the point made in the main text by showing more slices of the 3-dimensional parameter space of sterile neutrinos. We compare the MiniBooNE-preferred regions with exclusions from MicroBooNE, PROSPECT, and the sensitivity of SBN with and without PROSPECT-II in Fig. 5 using the global $\Delta\chi^2$ with 3 degrees of freedom, and assuming Wilks' theorem. The result of our coverage test is validated by noting that all MiniBooNE regions are already covered by MicroBooNE at the 95% CL level, even before including PROSPECT data.

In Fig. 6, we also show the event rates for MiniBooNE (top) and MicroBooNE ν_e sample (middle) and ν_μ sample (bottom), after subtraction of mis-ID backgrounds. For reference, we present the theory predictions of a sterile neutrino model for the two benchmark points shown in Figs. 2 and 3.

SBN sensitivities – To estimate the Asimov sensitivity of SBN, we use a χ^2 test statistic and model the systematic uncertainty on the BNB flux and neutrino-Argon cross sections via an approximate covariance matrix. We analyze the ν_μ and ν_e spectra of SBND and ICARUS to-

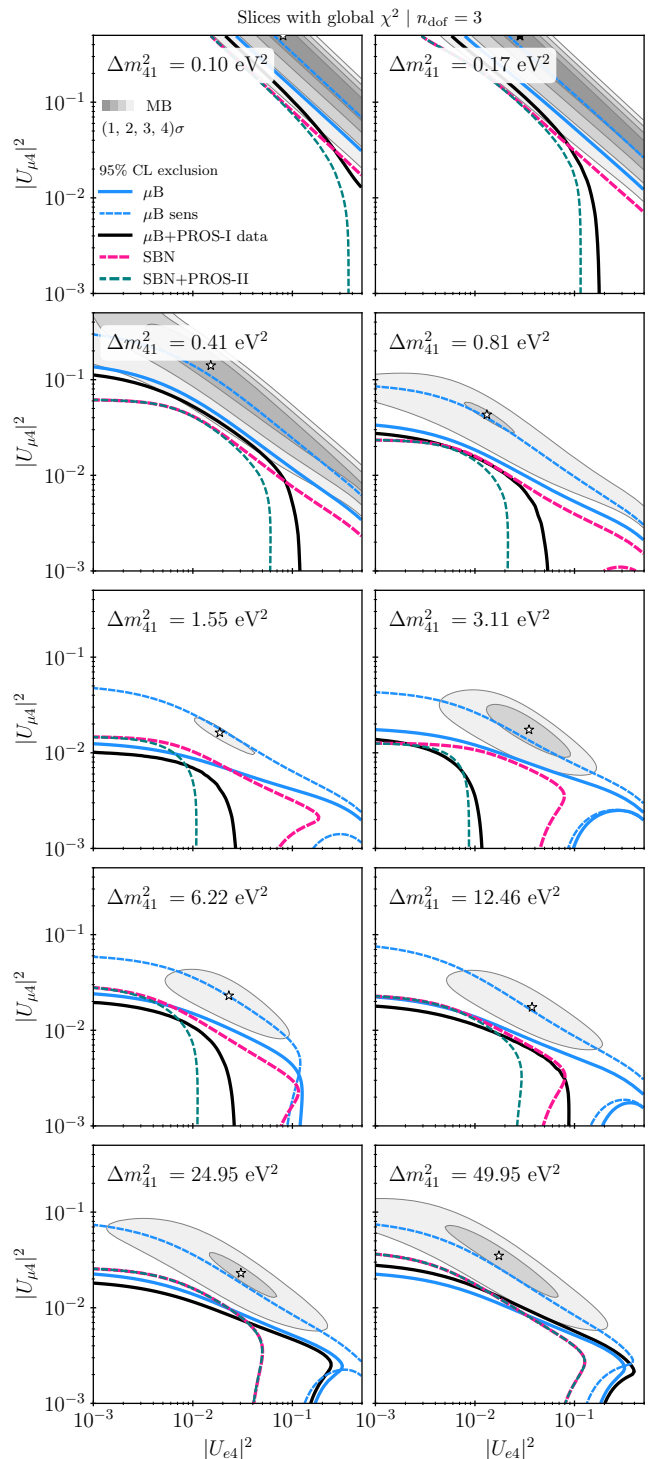


FIG. 5. The MiniBooNE preferred regions, MicroBooNE exclusion, and SBN sensitivities in slices of fixed Δm^2_{41} of the 3-dimensional parameter space of sterile neutrinos for 3 degrees of freedom (global χ^2). Excluded regions are to the top right of each panel.

gether. We account for energy-dependent cross section uncertainties $\sigma_i^{\text{XS}} = 15\%$, fully correlated between ν_μ and

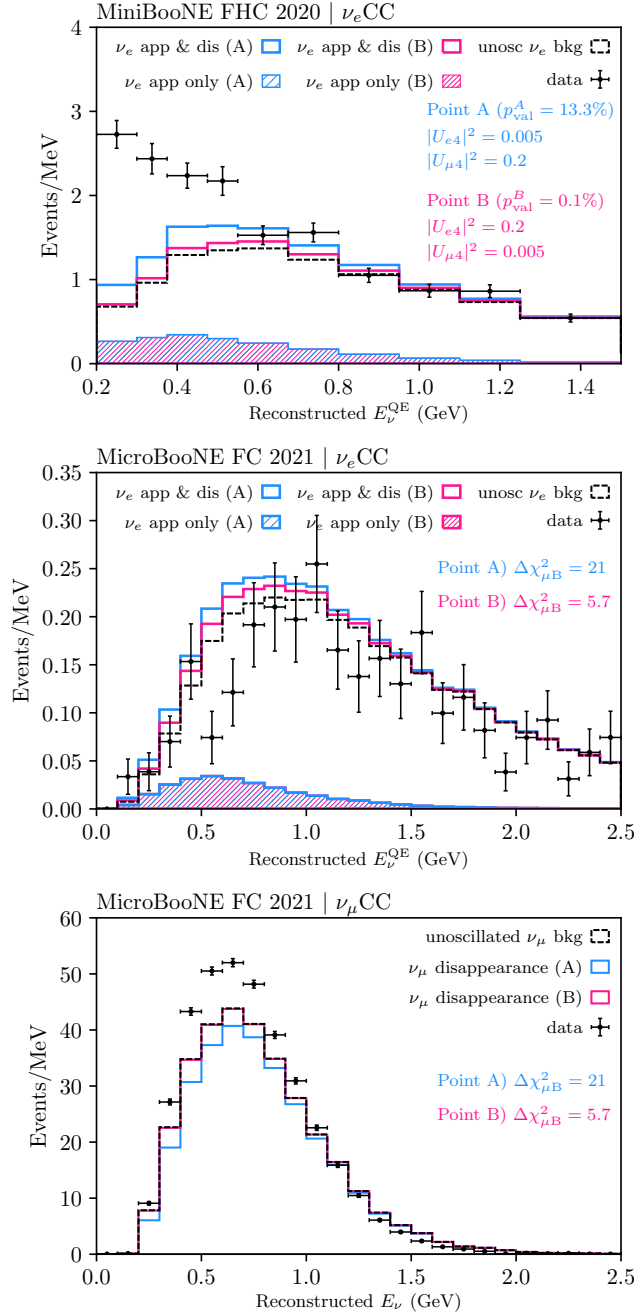


FIG. 6. The ν_e event rate at MiniBooNE (top) and MicroBooNE (middle), and ν_μ event rate at MicroBooNE (bottom), after subtraction of mis-ID backgrounds. We show the theory prediction of a sterile neutrino model for the two benchmark points discussed in Figs. 2 and 3, both with the same mass splitting $\Delta m_{41}^2 = 0.41 \text{ eV}^2$. Point A shows a point excluded by μB at the $\Delta\chi_{\mu\text{B}}^2 = 21$ level, and point B shows a point with the ν_e appearance/disappearance degeneracy that is compatible with μB at $\Delta\chi_{\mu\text{B}}^2 = 5.7$.

ν_e and between SBND and ICARUS, but uncorrelated over all energies E_i . For flux uncertainties, we take as the ν_e and ν_μ fluxes to be independent. We consider

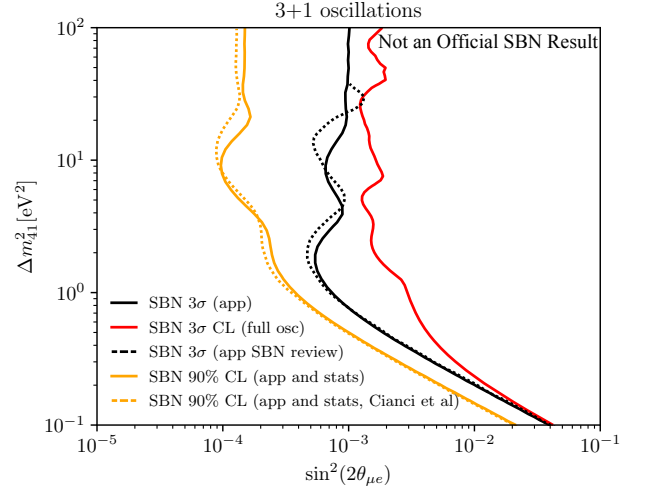


FIG. 7. The comparison of our SBN sensitivities with the literature for the case of a sterile model with $\nu_\mu \rightarrow \nu_e$ appearance only. We compare our sensitivity using statistical uncertainty only (solid orange) with that in Ref. [37] (dashed orange). We also compare the sensitivity including systematics (solid black) with that in Ref. [38]. Also shown is our sensitivity for a full oscillation model (solid red).

$\sigma_i^e = 10\%$, correlated among ν_e samples in both experiments but uncorrelated over all energies E_i , and similar for ν_μ .

For validation, we also show the 2-dimensional parameter space of Δm_{41}^2 vs $\sin^2(2\theta_{\mu e})$ in Fig. 7, comparing our result for the simpler, though unphysical, appearance-only model with that of Ref. [37] for the case of statistical uncertainties only, and with the one in Ref. [38] for the appearance-only full systematics case. No previous SBN sensitivity curve could be found for the case of full oscillations.

* obenevidesrodrigues@iit.edu

† mhostert@g.harvard.edu

‡ kjkelly@tamu.edu

§ blittlej@iit.edu

¶ pmachado@fnal.gov

** isafa94@gmail.com

†† taozhou@tamu.edu

- [1] A. A. Aguilar-Arevalo *et al.* (MiniBooNE), *Phys. Rev. D* **103**, 052002 (2021), arXiv:2006.16883 [hep-ex].
- [2] R. J. Hill, *Phys. Rev. D* **81**, 013008 (2010), arXiv:0905.0291 [hep-ph].
- [3] R. J. Hill, *Phys. Rev. D* **84**, 017501 (2011), arXiv:1002.4215 [hep-ph].
- [4] V. Brdar and J. Kopp, *Phys. Rev. D* **105**, 115024 (2022), arXiv:2109.08157 [hep-ph].
- [5] K. J. Kelly and J. Kopp, *JHEP* **05**, 113 (2023), arXiv:2210.08021 [hep-ph].
- [6] M. A. Acero *et al.*, (2022), arXiv:2203.07323 [hep-ex].

- [7] A. Aguilar *et al.* (LSND), *Phys. Rev. D* **64**, 112007 (2001), arXiv:hep-ex/0104049.
- [8] M. Dentler, A. Hernández-Cabezudo, J. Kopp, P. A. N. Machado, M. Maltoni, I. Martinez-Soler, and T. Schwetz, *JHEP* **08**, 010 (2018), arXiv:1803.10661 [hep-ph].
- [9] A. Diaz, C. A. Argüelles, G. H. Collin, J. M. Conrad, and M. H. Shaevitz, *Phys. Rept.* **884**, 1 (2020), arXiv:1906.00045 [hep-ex].
- [10] S. Böser, C. Buck, C. Giunti, J. Lesgourgues, L. Ludhova, S. Mertens, A. Schukraft, and M. Wurm, *Prog. Part. Nucl. Phys.* **111**, 103736 (2020), arXiv:1906.01739 [hep-ex].
- [11] R. Acciarri *et al.* (MicroBooNE, LAr1-ND, ICARUS-WA104), (2015), arXiv:1503.01520 [physics.ins-det].
- [12] P. Abratenko *et al.* (MicroBooNE), *Phys. Rev. Lett.* **128**, 111801 (2022), arXiv:2110.00409 [hep-ex].
- [13] P. Abratenko *et al.* (MicroBooNE), *Phys. Rev. Lett.* **128**, 241801 (2022), arXiv:2110.14054 [hep-ex].
- [14] P. Abratenko *et al.* (MicroBooNE), *Phys. Rev. D* **105**, 112005 (2022), arXiv:2110.13978 [hep-ex].
- [15] P. Abratenko *et al.* (MicroBooNE), *Phys. Rev. D* **105**, 112003 (2022), arXiv:2110.14080 [hep-ex].
- [16] P. Abratenko *et al.* (MicroBooNE), *Phys. Rev. D* **105**, 112004 (2022), arXiv:2110.14065 [hep-ex].
- [17] E. Wang, L. Alvarez-Ruso, and J. Nieves, *Phys. Lett. B* **740**, 16 (2015), arXiv:1407.6060 [hep-ph].
- [18] C. A. Argüelles, I. Esteban, M. Hostert, K. J. Kelly, J. Kopp, P. A. N. Machado, I. Martinez-Soler, and Y. F. Perez-Gonzalez, *Phys. Rev. Lett.* **128**, 241802 (2022), arXiv:2111.10359 [hep-ph].
- [19] P. B. Denton, *Phys. Rev. Lett.* **129**, 061801 (2022), arXiv:2111.05793 [hep-ph].
- [20] P. Abratenko *et al.* (MicroBooNE), *Phys. Rev. Lett.* **130**, 011801 (2023), arXiv:2210.10216 [hep-ex].
- [21] A. A. Aguilar-Arevalo *et al.* (MiniBooNE), (2021), arXiv:2110.15055 [hep-ex].
- [22] M. Hostert, K. J. Kelly, and T. Zhou, *Phys. Rev. D* **110**, 075002 (2024), arXiv:2406.04401 [hep-ph].
- [23] J. Ashenfelter *et al.* (PROSPECT), *Nucl. Instrum. Meth. A* **922**, 287 (2019), arXiv:1808.00097 [physics.ins-det].
- [24] M. Andriamirado *et al.* (PROSPECT), *Phys. Rev. D* **103**, 032001 (2021), arXiv:2006.11210 [hep-ex].
- [25] M. Andriamirado *et al.* (PROSPECT, (PROSPECT Collaboration)*), *Phys. Rev. Lett.* **131**, 021802 (2023), arXiv:2212.10669 [nucl-ex].
- [26] M. Andriamirado *et al.* (PROSPECT), (2024), arXiv:2406.10408 [hep-ex].
- [27] MicroBooNE Collaboration, *Updates to the NuMI Flux Simulation at MicroBooNE*, Tech. Rep. MICROBOONE-NOTE-1129-PUB (MicroBooNE, 2024).
- [28] MicroBooNE Collaboration, *Search for a Sterile Neutrino in a 3+1 Framework using Wire-Cell Inclusive Charged-Current ν_e Selection with the BNB and NuMI beamlines in MicroBooNE*, Tech. Rep. MICROBOONE-NOTE-1132-PUB (MicroBooNE, 2024).
- [29] P. Adamson *et al.* (MiniBooNE, MINOS), *Phys. Rev. Lett.* **102**, 211801 (2009), arXiv:0809.2447 [hep-ex].
- [30] P. Abratenko *et al.* (ICARUS), *Eur. Phys. J. C* **83**, 467 (2023), arXiv:2301.08634 [hep-ex].
- [31] P. Abratenko *et al.* (SBND), *Eur. Phys. J. C* **84**, 1046 (2024), arXiv:2406.07514 [physics.ins-det].
- [32] M. Andriamirado *et al.* (PROSPECT), *J. Phys. G* **49**, 070501 (2022), arXiv:2107.03934 [hep-ex].
- [33] K. Goldhagen, M. Maltoni, S. E. Reichard, and T. Schwetz, *Eur. Phys. J. C* **82**, 116 (2022), arXiv:2109.14898 [hep-ph].
- [34] F. P. An *et al.* (Daya Bay), *Phys. Rev. Lett.* **113**, 141802 (2014), arXiv:1407.7259 [hep-ex].
- [35] J. M. Berryman and P. Huber, *JHEP* **01**, 167 (2021), arXiv:2005.01756 [hep-ph].
- [36] C. Giunti, Y. F. Li, C. A. Ternes, and Z. Xin, *Phys. Lett. B* **829**, 137054 (2022), arXiv:2110.06820 [hep-ph].
- [37] D. Cianci, A. Furmanski, G. Karagiorgi, and M. Ross-Lonergan, *Phys. Rev. D* **96**, 055001 (2017), arXiv:1702.01758 [hep-ph].
- [38] P. A. Machado, O. Palamara, and D. W. Schmitz, *Ann. Rev. Nucl. Part. Sci.* **69**, 363 (2019), arXiv:1903.04608 [hep-ex].